Journal of the Iranian Chemical Society
https://doi.org/10.1007/s13738-024-03169-6

ORIGINAL PAPER

Design, molecular modelling, synthesis, characterization studies of novel N-(7-(substituted benzylidene)-4-phenyl-4,5,6,7-tetrahydro-3H-cyclopenta[d] pyrimidin-2-yl)-1-(substituted phenyl)methanimine against breast cancer

Arunkumar Manoharan[1] · Panneerselvam Theivendren[2] · Maya Sharma[1] · Selvaraj Kunjiappan[3] · Saravanan Govindaraj[2] · Parasuraman Pavadai[4]

Received: 15 July 2024 / Accepted: 30 December 2024

Abstract

A designed seventy-five distinct group of compounds namely N-(7-(substituted benzylidene)-4-phenyl-4,5,6,7-tetrahydro-3H-cyclopenta[d]pyrimidin-2-yl)-1-(substitutedphenyl) methanimine underwent evaluation for their potential against breast cancer utilizing various methods such as computational docking and dynamics, synthetic processes, structural characterization, and in vitro testing. The compound known as 2a3 was pinpointed through several analyses including elemental, HR-MS, FT-IR, ^{1}H NMR, and ^{13}C NMR. The online platform SwissADME predicted its physicochemical, drug-like, and pharmacokinetic profiles. Identification of drug targets was achieved using a network pharmacology technique, and extensive molecular docking tests were conducted to analyse how well the ligand and its complexes interacted with 23 specific breast cancer targets. These experiments revealed that the 2a3 complex demonstrated superior binding energy and interaction capabilities. Remarkably, 3LFF (Human p38 kinase), 5EW8 (Fibroblast growth factor receptor), 6E2N (MAPK), 6WW8 (CDK4/6 receptor), 7PCD (HER2), 7WT0 (human glyoxalase 1 receptor) and 8EXL (PI3K-alpha) showed outstanding binding energy and an amino acid interaction profile that stood out from the rest. The anticancer abilities of the synthesized compounds were assessed using the MTT assay, which showed that the compound 4-((2-((3-nitrobenzylidene)amino)-4-phenyl-3,4,5,6-tetrahydro-7H-cyclopenta [d]pyrimidin-7-ylidene) methyl) aniline 2a3 exhibited significant cytotoxic properties against MCF-7 cell lines. Given their highly effective performance in cellular environments, the compound 2a3, hold IC_{50} value of 14.03 µM/mL against MCF-7 cells and it's a potential in the advancement of more effective treatments against cancer cell proliferation.

Graphical abstract

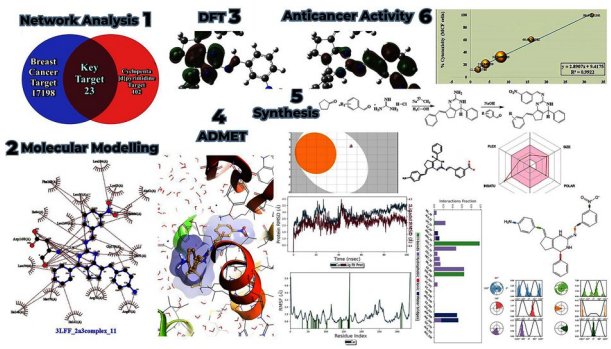

Keywords Cyclopenta[d]pyrimidin · Schiff bases · Molecular Modelling · ADMET studies · Cytotoxicity

Extended author information available on the last page of the article

Published online: 17 January 2025

Introduction

Cancer persists as a significant public health issue globally, impacting the lives of millions. Conventional therapies like chemotherapy and radiotherapy often encounter limitations due to multidrug resistance (MDR), prompting ongoing research into new substances that can combat cancer effectively [1, 2]. Pyrimidines, known for their broad biological and pharmacological functions, have garnered significant interest. Fused pyrimines, a subclass of heterocyclic compounds, are extensively studied in medicinal chemistry for their promising anticancer properties [3, 4]. The foundational pyrimidine ring, prevalent in many biological molecules such as nucleotides, vitamins, and coenzymes, facilitates the creation of various derivatives with potent anticancer qualities. Pyrimidine, characterized by a six-membered heterocyclic ring containing nitrogen at the first and third positions, is crucial in numerous biomolecules, including nucleotides, nucleic acids (DNA and RNA), vitamins, and coenzymes. It is noteworthy in cancer research due to its analogy with nucleotide bases in DNA and RNA [5, 6]. Fused pyrimines disrupt cancer cell multiplication and transcription by mimicking these nucleotide bases, which is vital for hindering tumour growth and spread. Over the years, many novel pyrimidine derivatives have been synthesized, and their anticancer potential has been evaluated through various in vitro and in vivo techniques [7]. Fused pyrimines are particularly notable for their synthetic flexibility, allowing for the development of diverse structures by altering groups attached to the pyrimidine ring. These modifications have resulted in derivatives with improved cytostatic activities, which can halt the cell cycle and trigger apoptosis in cancer cells [8]. Among these, fused pyrimines, which integrate a cyclopentane ring into the pyrimidine structure, have proven effective against several cancer cell lines and show promise in surmounting MDR [9]. Prominent examples of drugs containing cyclopenta pyrimidine include zidovudine, stavudine, 5-fluorouracil, methotrexate, and imatinib. Intensive research into the structure–activity relationship (SAR) of these compounds has shown that specific modifications, notably the addition of electron-withdrawing groups to the aryl component connected to the pyrimidine ring [10], significantly enhance their antiproliferative actions, whereas electron-donating groups may diminish their effectiveness [11]. Recent efforts in the field continue to focus on developing pyrimidine derivatives that possess high anticancer activity, favourable pharmacokinetic profiles, and minimal adverse effects, such as gemcitabine and 5-fluorouracil. Pyrido[2,3-d]pyrimidines, a subtype of cyclopenta pyrimidines, display a range of effects, including antitumor, antibacterial, and analgesic properties [12, 13]. Products like Palbociclib, a CDK4/6 inhibitor for breast cancer treatment, incorporate the pyrido[2,3-d]pyrimidine structure. The ongoing research underscores the significant role of medicinal chemistry in evolving simple molecular frameworks into potent, life-saving therapies. The quest to develop more effective and selective cyclopyrimidine-based treatments is vital in combating cancer, providing new hope for patients worldwide. However, developing cyclopyrimidine for oncological use is complex due to drug resistance in cancer cells, necessitating the search for new agents with distinct mechanisms of action. The broad potential for structural modifications in pyrimidines aids in creating a variety of derivatives, though determining those with strong anticancer properties involves extensive exploration and testing. In addition, employing biomarkers to foresee therapeutic response or resistance adds complexity to the development process. It requires tailored approaches to match each patient's cancer's unique clinical and molecular features. Overall, these challenges notwithstanding, the ongoing advancements in creating and understanding cyclopyrimidine derivatives promise a brighter future in cancer treatment. The strategic optimization of their characteristics could lead to the advent of effective new therapies, further advancing the field of oncology.

Results and discussion

Target identification

The compounds N-(7-(substituted benzylidene)-4-phenyl-4,5,6,7-tetrahydro-3H-cyclopenta [d]pyrimidin-2-yl)-1-(substituted phenyl) methenamine were evaluated for their efficacy in combatting breast cancer. This analysis used Venn diagrams to examine the intersection between the targets of the drug and those affected by the disease. Resources such as Genecards, OMIM, and Swiss target prediction were employed to gather relevant target data. Venn diagrams, depicted as overlapping circles, serve as an effective visual technique to represent and analyse various data sets. In the context of breast cancer, these diagrams facilitate identifying and differentiating groups, showcasing the relationships and differences between markers or genetic mutations associated with the disease. Areas, where the circles intersect, might indicate shared properties or unique distinctions, helping to pinpoint 23 key targets for possible treatment or more in-depth study Fig. 1. An integrated graphical network presents these identified targets, allowing further evaluation to determine the most impactful targets for advancing breast cancer therapies. The identified targets include: TACE, Human p38 kinase, Renin complex, VEGF receptor, Progesterone receptor, Fibroblast growth factor receptor, KEAP 1, Human

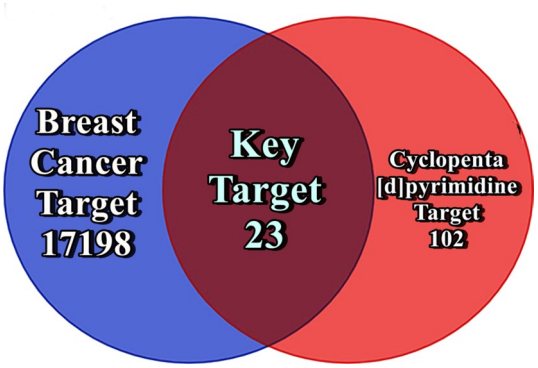

Fig. 1 Graphical representations of Venn diagram for cyclopenta[d] pyrimidine, breast cancer and common targets

PARP inhibitor, Transthyretin receptor, Oestrogen receptor, MAPK, Carboxypeptidase A1 receptor, Bcl-2 receptor, Carbonic anhydrase IX, Tubulin alpha receptor, CDK4/6 receptor, PYCR1, HER2, human glyoxalase 1 receptor, oestrogen receptor beta, EGFR. ER-alpha, PI3K-alpha.

In silico modelling

Molecular docking studies of seventy-five compounds of N-(7-(substituted benzylidene)-4-phenyl-4,5,6,7-tetrahydro-3H-cyclopenta[d]pyrimidin-2-yl)-1-(substitutedphenyl) methanimine, along with the cocrystals namely 3WEJ (TACE), 5GIT (KEAP 1), 3VUC (Renin complex), 3WZE (VEGF receptor), 3ZR7 (Progesterone receptor), 5EW8 (Fibroblast growth factor receptor), 5LX6 (Human PARP inhibitor), 5U49 (Transthyretin receptor), 5WGD (Oestrogen receptor), 6E2N (MAPK), 6I6Z (Carboxypeptidase A1 receptor), 6QGG (Bcl-2 receptor), 6QUT (Carbonic anhydrase IX), 6S8L (Tubulin alpha receptor), 6WW8 (CDK4/6 receptor), 6XP1 (PYCR1), 7PCD (HER2), 7WT0 (human glyoxalase 1 receptor), 7XVZ (oestrogen receptor beta), 8A27 (EGFR), 8BWJ (ER-alpha), and 8EXL (PI3K-alpha). Among all, the following proteins 3LFF, 5EW8, 6E2N, 6WW8, 7PCD, 7WT0 and 8EXL with 2a3 complexes exhibit significant activity against the breast cancer that with the binding energy of − 11.5, − 11.0, − 10.3, − 10.9, − 11.1, − 7.4, and − 10.1 kcal × mol^{-1} respectively. Among the tested ligands including cocrystals, the compound 4-((2-((3-nitro benzylidene) amino)-4-phenyl-3,4,5,6-tetrahydro-7H-cyclopenta[d]pyrimidin-7-ylidene) methyl) aniline 2a3 showed high amino acid interaction and significant binding affinity towards 3LFF (Human p38 kinase), 5EW8 (Fibroblast growth factor receptor), 6E2N (MAPK), 6WW8 (CDK4/6 receptor), 7PCD (HER2), 7WT0 (human glyoxalase 1 receptor) and 8EXL (PI3K-alpha) proteins. In the 3LFF_2a3 complex, amino acids Arg67(A), Arg70(A), Chi71(A), Leu74(A), Met78(A), Ile141(A), Ile146(A), and Gly170(A) showed the most significant interactions with 2a3. Similarly, in the 5EW8_2a3 complex, Gly490(A), Leu644(A), Lys514(A), Gly487(A), Asp641(A), Glu531(A), Met535(A), Val492(A), Ile545(A), Ala512(A), Val561(A), Leu48(A), Ala564(A), Tyr563(A), and Leu630(A) also demonstrated substantial interactions. In the 6E2N_2a3 complex, prominent interactions were noted with Lys827(A), Thr840(A), Thr836(A), Arg802(A), Glu837(A), Phe839(A), Tyr858(A), and Lys853(A). For the 6WW8_2a3 complex, the amino acids interacting the most were Tyr197(A), Cys136(A), Met132(A), CEMetl05(A), Pro82(A), Phe83(A), Val87(A), Leu94(A), Asp88(A), Leu92(A), Lys91(A), Gln85(A), and Trp81(A). The 7PCD_2a3 complex saw significant interactions from Ala771(A), Phe64(A), Arg784(A), Ser783(A), Glu770(A), Thi862(A), Leu785(A), Thr798(A), Asp863(A), Thr798(A) again, Lys753(A), Val734(A), and Leu726(A). Additionally, in the 7WT0_2a3 complex, the amino acids that interacted most extensively were Arg122(A), Asn18(A), His126(A), Glu72(A), Leul60(A), Phe162(A), Trp170(A), Vall49(A), and Lys150(A). Lastly, in the 8EXL_2a3 complex, the amino acids Glu49(A), Phe930(A), Tyr836(A), Val51(A), Ile48(A), Asp933(A), Ser54(A), Gln59(A), His855(A), Arg770(A), Met922(A), Tip780(A), Met772(A), Pro-778(A), and Lys802(A) were the most interactively involved with 2a3. The binding interactions, 2D and 3D models of 2a3, are shown in Figs. 2 and 3. Further, the docking results value of the complexes were given in a supplementary file 1.

Molecular dynamics (MD)

The study was carried out to examine and clarify the interactions patterns displayed by the protein–ligand complexes of the 3LFF (Human p38 kinase), 5EW8 (Fibroblast growth factor receptor), 6E2N (MAPK), 6WW8 (CDK4/6 receptor), 7PCD (HER2), 7WT0 (human glyoxalase 1 receptor) and 8EXL (PI3K-alpha) proteins with 4-((2-((3-nitrobenzylidene)amino)-4-phenyl-3,4,5,6-tetrahydro-7H-cyclopenta[d]pyrimidin-7-ylidene) methyl) aniline 2a3 ligand. The root mean square deviation (RMSD) and root mean square fluctuation (RMSF) were systematically determined for the protein–ligand complex. Analysis of the RMSD and RMSF in relation to amino acid residues enabled the evaluation of the critical impacts of protein–ligand interactions and interaction fingerprints on the stability of the complex. Specifically, the protein–ligand complex of 4-((2-((3-nitrobenzylidene)amino)-4-phenyl-3,4,5,6-tetrahydro-7H-cyclopenta[d]pyrimidin-7-ylidene) methyl) aniline 2a3 was assessed by precisely measuring scale values of both proteins and ligands. The observed showed that the scale values of 3LFF_2a3 complex (Protein RMSD 4A° and Ligand RMSD 4.5A°), 5EW8_2a3 complex (Protein RMSD 3.2A° and Ligand RMSD 8A°), 6E2N_2a3 complex (Protein

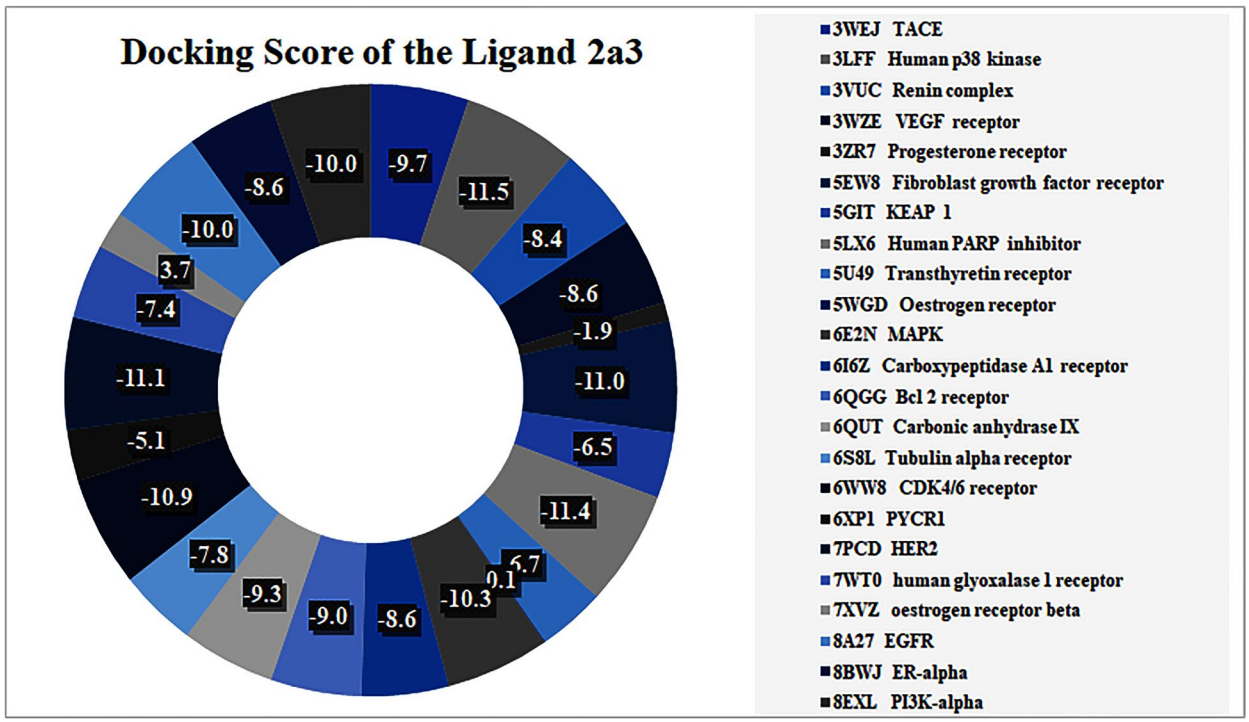

Fig. 2 The Docking Scores of 2a3 with 23 Protein Complex's

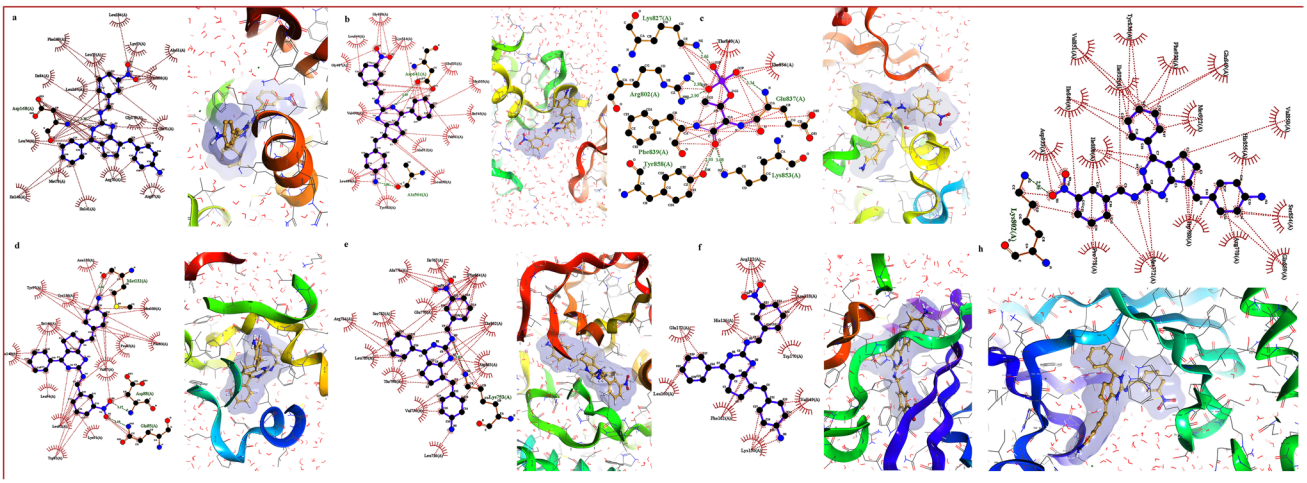

Fig. 3 The binding interactions, 2D and 3D model of 2a3 and 3LLF complex **a**, 2a3 and 5EW8 complex **b**, 2a3 and 6E2N complex **c**, 2a3 and 6WW8 complex **d**, 2a3 and 7PCD complex **e**, 2a3 and 7WT0 complex **f**, and 2a3 and 8EXL protein complex **g**

RMSD 24A° and Ligand RMSD 48A°), 6WW8_2a3 complex (Protein RMSD 2.4A° and Ligand RMSD 3.2A°), 7PCD_2a3 complex (Protein RMSD 3.6A° and Ligand RMSD 3.6A°), 7WT0_2a3 complex (Protein RMSD 13.5A° and Ligand RMSD 13.5A°) and 8EXL_2a3 complex (Protein RMSD 3.6A° and Ligand RMSD 5.6A°) proteins were acquired over a 100 ns MD production run. During the molecular dynamic simulation, the proteins 3LFF, 5EW8, 6E2N, 6WW8, 7PCD, 7WT0 and 8EXL-ligand 2a3 complexes were showed constant RMSF values. Throughout the MD simulation, it was observed that the fluctuation curve indicates constant interaction of 21 amino acids in 3LFF_2a3 complex, 47 amino acids in 5EW8_2a3 complex, 32 amino acids in 6E2N_2a3 complex, 17 amino acids in 6WW8_2a3 complex, 48 amino acids in 7PCD_2a3 complex, 22 amino acids in 7WT0_2a3 complex and 41 amino acids in 8EXL_2a3 complex, more over there was no fluctuation involved in the complexes, and the other amino

acids in the residual index of RMSF did not show fluctuation and all the complexes had good stability. The amino acid interaction in docking and MD simulation indicates in the 3LFF_2a3complex, Arg67(A), Arg70(A), Chi71(A), Leu74(A), Met78(A), Ile141(A), Ile146(A), and Gly170(A). 5EW8_2a3complex, amino acids that demonstrated a substantial degree of interaction include Gly490(A), Leu644(A), Lys514(A), Gly487(A), Asp641(A), Glu531(A), Met535(A), Val492(A), Ile545(A), Ala512(A), Val561(A), Leu48(A), Ala564(A), Tyr563(A), and Leu630(A). In the case of 6E2N_2a3complex, Lys827(A), Thr840(A), Thr836(A), Arg802(A), Glu837(A), Phe839(A), Tyr858(A), and Lys853(A). For the complex labelled 6WW8_2a3complex, Ty197(A), Cys136(A), Met132(A), Met105(A), Pro82(A), Phe83(A), Val87(A), Leu94(A), Asp88(A), Leu92(A), Lys91(A), Gln85(A), and Trp81(A). In 7PCD_2a3complex, Ala771(A), Phe64(A), Arg784(A), Ser783(A), Glu770(A), Thi862(A), Leu785(A), Thr798(A), Asp863(A), Lys753(A), Val734(A), and Leu726(A). The key interacting amino acids included 7WT0_2a3complex, Arg122(A), Asn18(A), His126(A), Glu72(A), Leu160(A), Phe162(A), Trp170(A), Val149(A), and Lys150(A). The prevalent interactions were observed with 8EXL_2a3complex, Glu49(A), Phe930(A), Tyr836(A), Val51(A), Ile48(A), Asp933(A), Ser54(A), Gln59(A), His855(A), Arg770(A), Met922(A), Tip780(A), Met772(A), Pro778(A), and Lys802(A). The docking interaction of 2a3 indicates that the amino acid interaction was consistent with the MD simulation interaction. In this illustration, the angular coordinate represents the torsional angle, and the radial coordinate represents the torsion potential of the rotatable bond. The rigid bonds and flexible bonds of 3LFF_2a3 complex, 5EW8_2a3 complex, 6E2N_2a3 complex, 6WW8_2a3 complex, 7PCD_2a3 complex, 7WT0_2a3 complex and 8EXL_2a3 complex, were shown in their structures Figs. 4, 5 and 6 and Supplementary file 1.

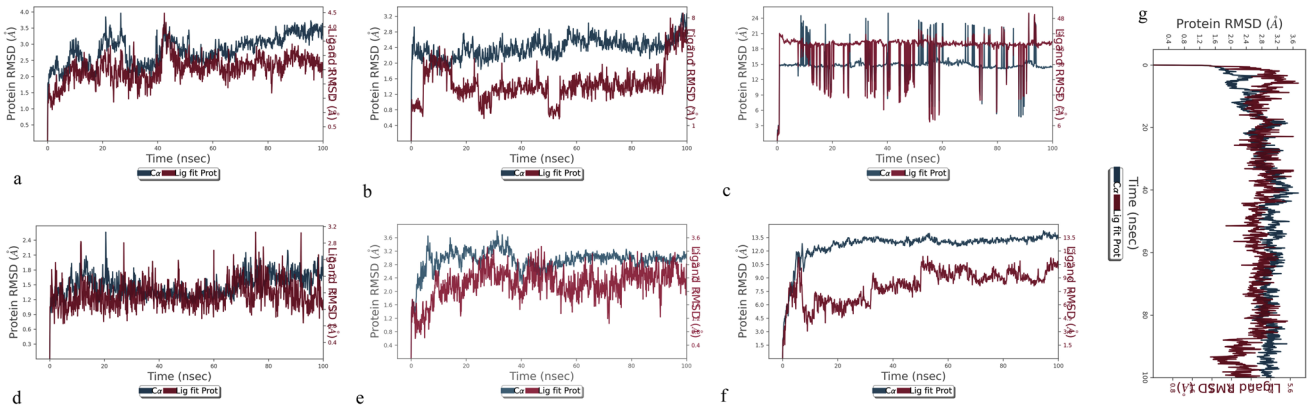

Fig. 4 RMSD of 2a3 and 3LLF complex **a**, 2a3 and 5EW8 complex **b**, 2a3 and 6E2N complex **c**, 2a3 and 6WW8 complex **d**, 2a3 and 7PCD complex **e**, 2a3 and 7WT0 complex **f** and 2a3 and 8EXL protein complex **g**

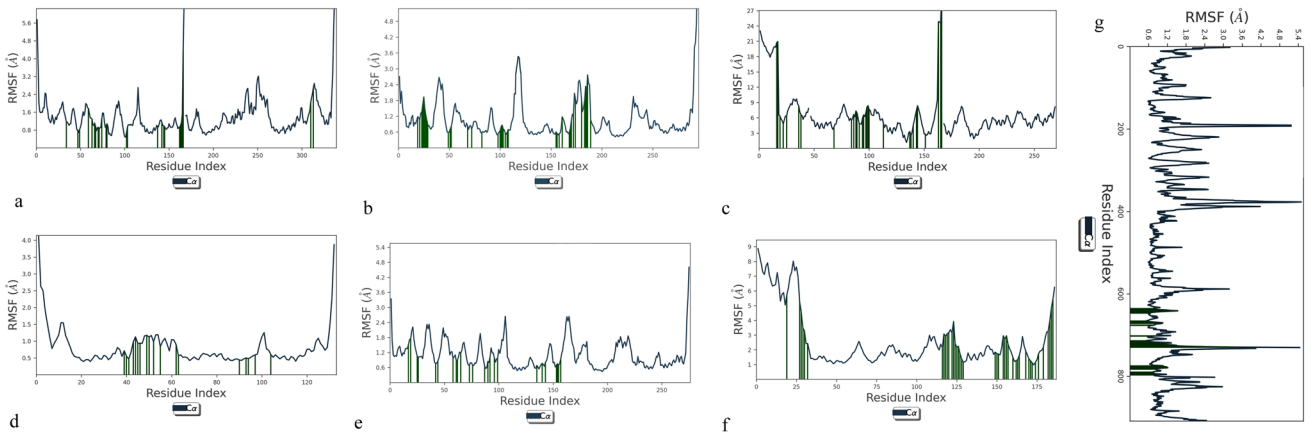

Fig. 5 RMSF of 2a3 and 3LLF complex **a**, 2a3 and 5EW8 complex **b**, 2a3 and 6E2N complex **c**, 2a3 and 6WW8 complex **d**, 2a3 and 7PCD complex **e**, 2a3 and 7WT0 complex **f** and 2a3 and 8EXL protein complex **g**

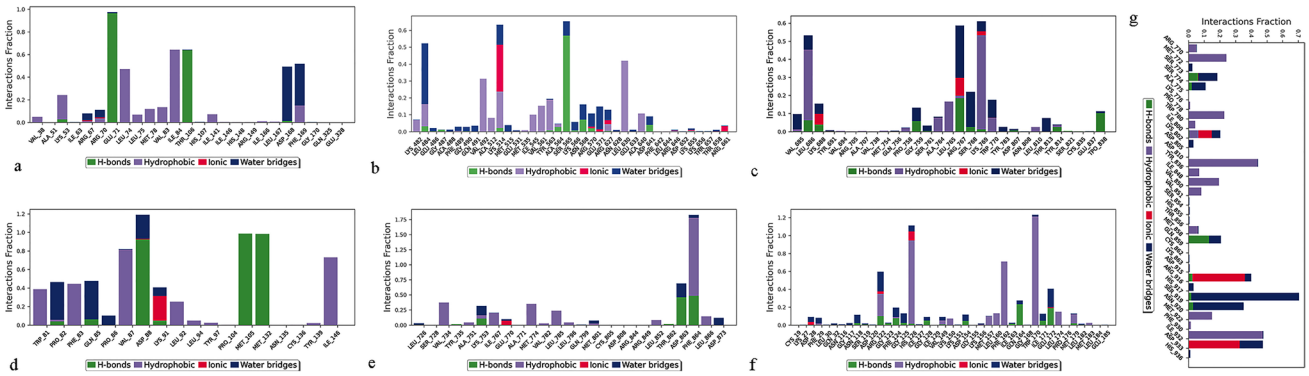

Fig. 6 Protein–ligand contacts 2a3 and 3LLF complex **a**, 2a3 and 5EW8 complex **b**, 2a3 and 6E2N complex **c**, 2a3 and 6WW8 complex **d**, 2a3 and 7PCD complex **e**, 2a3 and 7WT0 complex **f**, and 2a3 and 8EXL protein complex **g**

Density functionality theory

The HOMO and LUMO energy values were used to determine the stability and confirm the bioactive qualities of the active substances 2a3. These values facilitated the computation of the energy gap, which in turn was crucial for evaluating the compounds' stability and bioactivity. For the active ingredient 2a3, the HOMO and LUMO energy gap was recorded at 2.0416. The findings indicate that 2a3 has notable stability. Figure 7 displays the energy levels for the HOMO and LUMO of 2a3.

ADMET prediction

The SwissADME web server assessed the ADME and physicochemical characteristics of the active molecule 2a3. The examination revealed that the molecule's polar surface area is 108.59 A^2, exhibiting a high gastrointestinal absorption rate. Generally, enhanced absorption in the stomach can lead to increased chemical bioavailability. Thus, administering 2a3 orally may improve its absorption through the gastrointestinal tract. The binding mechanism between the protein and ligand will involve five rotatable bonds, four hydrogen bond acceptors, and two hydrogen bond donors. The bioavailability index of 2a3 stood out at + 0.55. Molecular investigations revealed that 2a3 has a synthetic accessibility score of 4.85. According to Fig. 8, there are no violations of Lipinski's rule for 2a3, depicted by a pink area in the hexagon indicating the optimal compound range, and saturation levels are ideal for drug-like properties. Under the Sp3 hybridization rule, 25% of the carbon atoms should be present, and for a compound to be considered insoluble, it must have a log S value below 6. Hydrophobicity should range from − 0.7 to + 5.0, and rotatable bonds should not exceed nine. The molecular mass should fall between 150 and 500 $g.mol^{-1}$. Drug-like reference compounds are indicated by a red-slanted hexagon against a pink background for the polar surface area. Figure 8 demonstrates

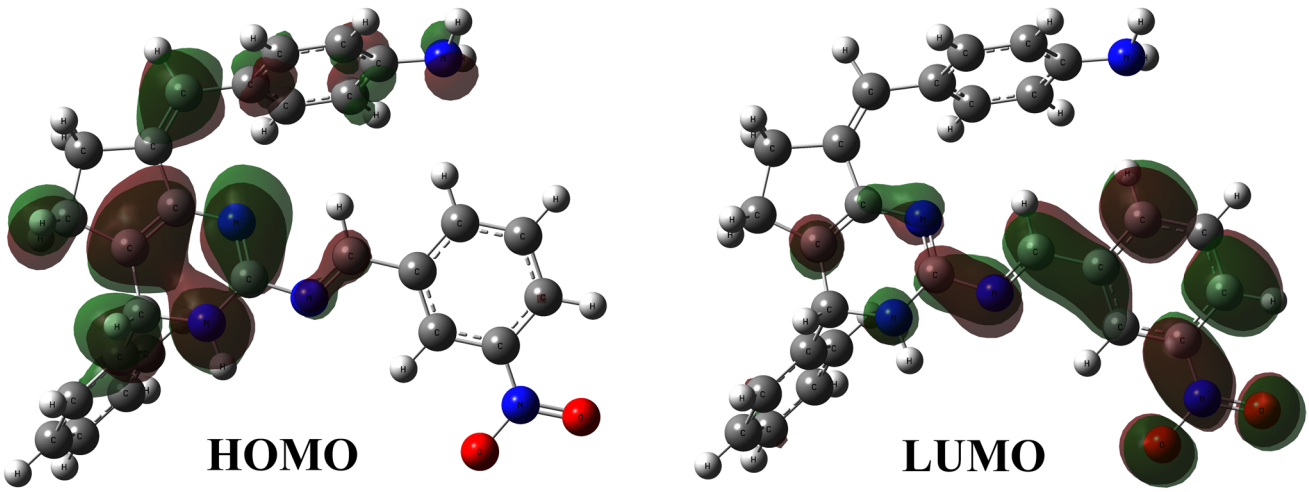

Fig. 7 The energy values of HOMO and LUMO of 2a3

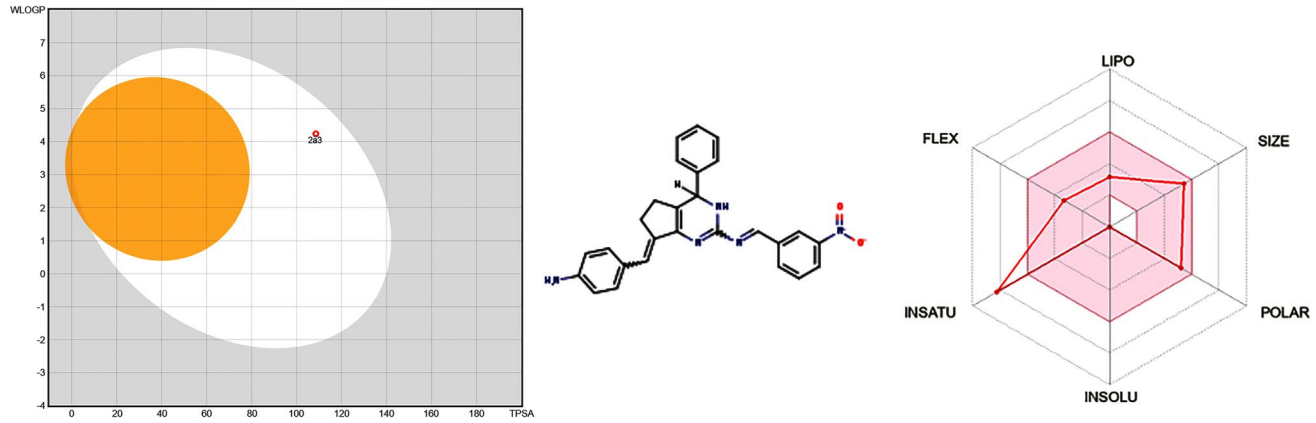

Fig. 8 The Lipinski properties and egg-boiled model of 2a3

two critical pharmacokinetic properties analysed using an egg-boiled model, assessing both passive gastrointestinal absorption and the capability to penetrate the blood–brain barrier. The visuals confirm that the yolk substance can cross the blood–brain barrier, while the albumin is more likely absorbed in the stomach. Compound 2a3, shown in white in Fig. 8, had gastric solid absorption, signalling its potential as an effective active agent. The primary metabolic site for compound 2a3 was predicted using SMARTCyp, which identified that the compound underwent metabolism primarily through dealkylation and deamination. The first and second metabolites were traced back to the pyrimidine group within the structure of 4-((2-((3-nitrobenzylidene)amino)-4-phenyl-3,4,5,6-tetrahydro-7H-cyclopenta[d]pyrimidin-7-ylidene) methyl) aniline 2a3. Additionally, the third metabolite originated from the NH_2 group in the structure of 2a3, as shown in Fig. 9. The cardiotoxicity for compound 2a3 was predicted using Cardio TaxCSM, which identified that the compound 2a3 has safe Arrhythmia, Cardiac_Failure, Heart_Block, Hypertension and Myocardial_Infaction.

Synthesis

7-Benzylidene-4-phenyl-4,5,6,7-tetrahydro-3H-cyclopenta[d]pyrimidin-2-amine (I)

Yield (%): 78; m.p. (°C): 134–136. IR (cm^{-1}): 3359 (NH), 3014 (Ar–CH), 2907 (CH_2–CH), 1652 (C = N), 1605 (C = C). ^{1}H–NMR (δ: ppm): 6.83–7.90 (10H, m, Ar–CH), 6.48 (1H, s, = CH), 5.36 (s, 2H, NH_2) 5.32 (1H, s, NH), 4.75 (1H, s, CH of pyrimidine), 2.19 (2H, t, CH_2 of cyclopentane), 2.13 (2H, t, CH_2 of cyclopentane). ^{13}C–NMR (δ: ppm): 158.5 (C-2), 145.8 (C”-1), 142.2 (C-7), 137.0 (C’-1), 136.4 (C-7a), 134.7 (C-5a), 130.5 (C’-3 & C’-5), 129.9 (C’-2 & C’-6), 129.3 (C”-3 & C”-5), 128.6 (C’-4), 126.5 (C”-2 & C”-6), 126.0 (C”-4), 122.8 (C = CH), 64.1 (C-4), 31.4 (C-5), 24.7 (C-6). MS (EI) *m/z*: 301 (M^+). *Anal*. Calcd for $C_{20}H_{19}N_3$: C, 79.70; H, 6.35; N, 13.94. Found: C, 79.96; H, 6.33; N, 13.90.

4-((2-((3-nitrobenzylidene)amino)-4-phenyl-3,4,5,6-tetrahydro-7*H*-cyclopenta[*d*]pyrimidin-7-ylidene)methyl)aniline (2a3)

Yield (%): 74; m.p. (°C): 216–218. IR (cm^{-1}): 3281 (NH), 3005 (Ar–CH), 2879 (CH_3-CH), 1632 (C = N), 1617 (C = C), 1513 & 1336 (NO_2). ^{1}H-NMR (δ: ppm): 8.69 (1H, s, N = CH), 7.13–8.24 (13H, m, Ar–CH), 6.36 (1H, s, = CH), 5.45 (s, 2H, NH_2), 5.12 (s, 2H, NH_2), 5.08 (1H, s, NH), 4.50 (1H, s, CH of pyrimidine), 2.25 (2H, t, CH_2 of cyclopentane), 2.22 (2H, t, CH_2 of cyclopentane). ^{13}C-NMR (δ: ppm): 167.5 (N = CH), 152.1 (C-2), 151.9 (C’”-3), 149.3 (C’-4), 138.7 (C”-1), 138.0 (C-7), 136.8 (C’”-6), 135.5 (C-7a), 133.2 (C’”-1), 130.6 (C-5a), 127.1 (C’”-5), 126.9 (C’-2 & C’-6), 126.4 (C”-3 & C”-5), 125.0 (C”-2 & C”-6), 123.3 (C”-4), 122.8 (C’”-4), 121.5 (C’-1), 121.1 (C = CH), 117.2 (C’”-2), 110.6 (C’-3 & C’-5), 56.4 (C-4), 25.9 (C-5), 21.2 (C-6). MS (EI) *m/z*: 449 (M^+). *Anal*. Calcd for $C_{27}H_{23}N_5O_2$: C, 72.14; H, 5.16; N, 15.58. Found: C, 71.92; H, 5.18; N, 15.63.

Chemistry

This study developed a series of novel compounds by starting with 7-benzylidene-4-phenyl-4,5,6,7-tetrahydro-3H-cyclopenta[d] pyrimidin-2-amine (I). This precursor underwent a Schiff base reaction, where it was treated with different aromatic aldehydes in the presence of sodium acetate within an environment of glacial acetic acid. This process yielded N-(7-(substituted benzylidene)-4-phenyl-4,5,6,7-tetrahydro-3H-cyclopenta[d]pyrimidin-2-yl)-1-(substituted phenyl) methanimine derivatives. Throughout

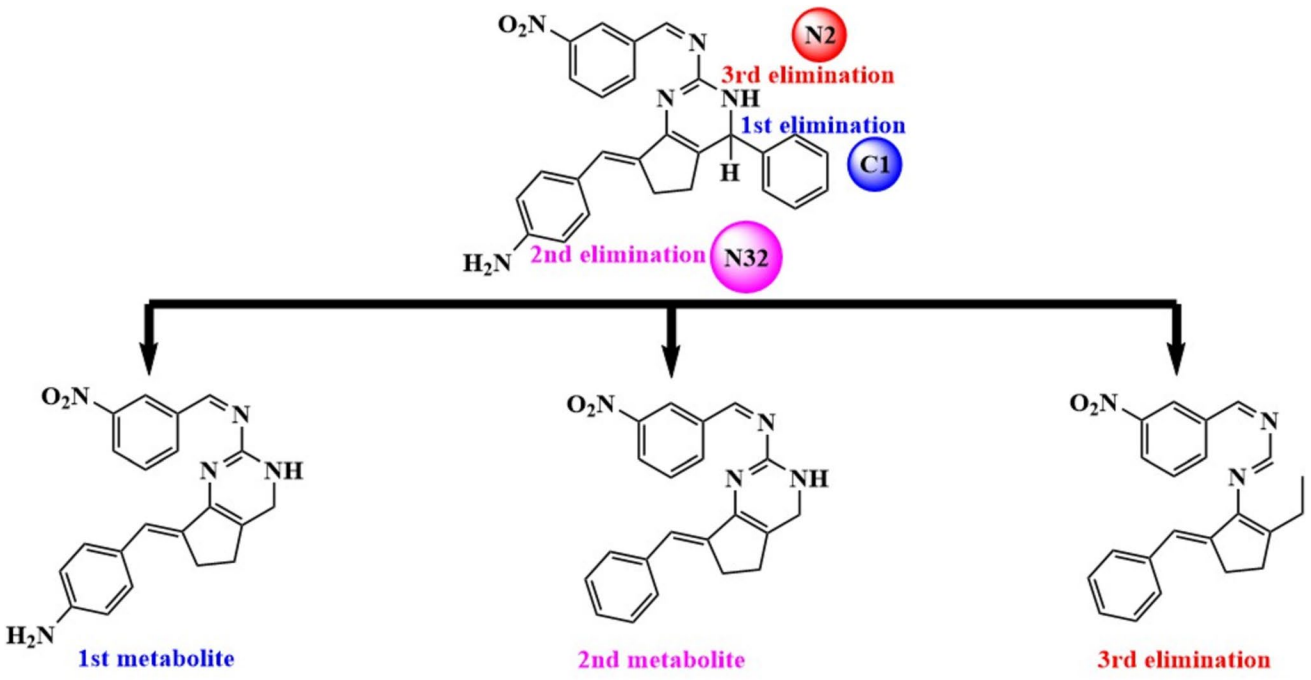

Atom	Scores of Cytochrome P450 3A4, 2D6 and 2C9 isoform		
	3A4	2D6	2C9
C1	36.3	51.9	51.9
N32	43.9	71.7	64.5
N2	48.6	71.7	70.1

Fig. 9 The Scores of Cytochrome P450 3A4, 2D6 and 2C9 isoform and metabolic pathway of 2a3

the synthesis, thin-layer chromatography (TLC) was utilized to monitor and verify the completion of the reactions and assess the purity of the products. The formation of the derivatives was indicated by specific infrared (IR) absorption peaks. Peaks between 3281 and 3385 cm^{-1} and 1632–1650 cm^{-1} were observed, which are descriptive of NH and C = N stretchings, respectively. Further spectroscopic support for forming these compounds came from additional IR absorption peaks. Peaks in the 3005–3021 cm^{-1}, 2879–2936 cm^{-1}, and 1603–1625 cm^{-1}, correspond to Ar–CH, CH_2–CH, and C = C stretchings respectively. Moreover, nuclear magnetic resonance (NMR) spectroscopy provided critical insights. The disappearance of the two-proton singlet at around δ 5.19 ppm, which is typically linked to NH_2 protons, and the emergence of a one-proton singlet in the δ 8.43–8.69 ppm range, characteristic of the –N = CH– proton, confirmed the successful synthesis. Further confirmation was provided by the ^{13}C–NMR, where a prominent peak emerging around δ 160.3–170.4 ppm correlative to the –CH = N– carbon was noted. Additionally, the presence of various other peaks in the IR, ^{1}H–NMR, and ^{13}C–NMR spectra corroborated the structural assignments of these derivatives. Finally, the molecular weight and purity of the newly synthesized analogue was validated via their mass spectra, ensuring that the compound met the criteria for clinical research use.

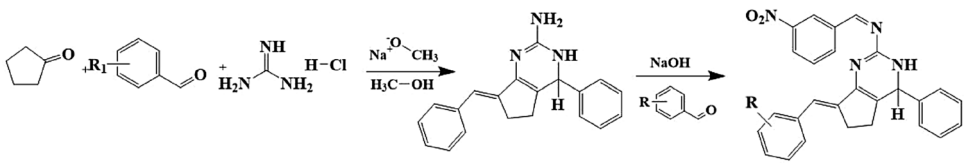

In vitro anti-breast cancer activity

The cytotoxicity assay is an important first stage in the discovery of novel anticancer drugs. The MTT assay was performed to determine the in vitro cytotoxic potential of compound 4-((2-((3-nitrobenzylidene)amino)-4-phenyl-3,4,5,6-tetrahydro-7H-cyclopenta[d]pyrimidin-7-ylidene) methyl) aniline 2a3 against the MCF-7 cells (breast cancer cells). The most relevant information gained from it is the change in the number of living and dead cells following 2a3 treatment. The displayed the percentage of cytotoxicity achieved by the MCF-7 cells after being treated with the test chemical. It was observed that the compound 2a3 had the significant cytotoxicity against the MCF-7 cells. Figure 4 demonstrated the results of the MTT assay showing the cytotoxic efficacy after being treated with compound 2a3. Further, the compound 4-((2-((3-nitrobenzylidene)amino)-4-phenyl-3,4,5,6-tetrahydro-7H-cyclopenta[d]pyrimidin-7-ylidene) methyl) aniline 2a3 exhibited an IC_{50} value of 14.03 µM/mL against MCF-7 cells and the anticancer results of the 2a3 was given in a Fig. 10.

Conclusion

The synthesis method developed for creating a new derivative, 4-((2-((3-nitrobenzylidene) amino)-4-phenyl-3,4,5,6-tetrahydro-7H-cyclopenta[d] pyrimidin-7-ylidene) methyl)

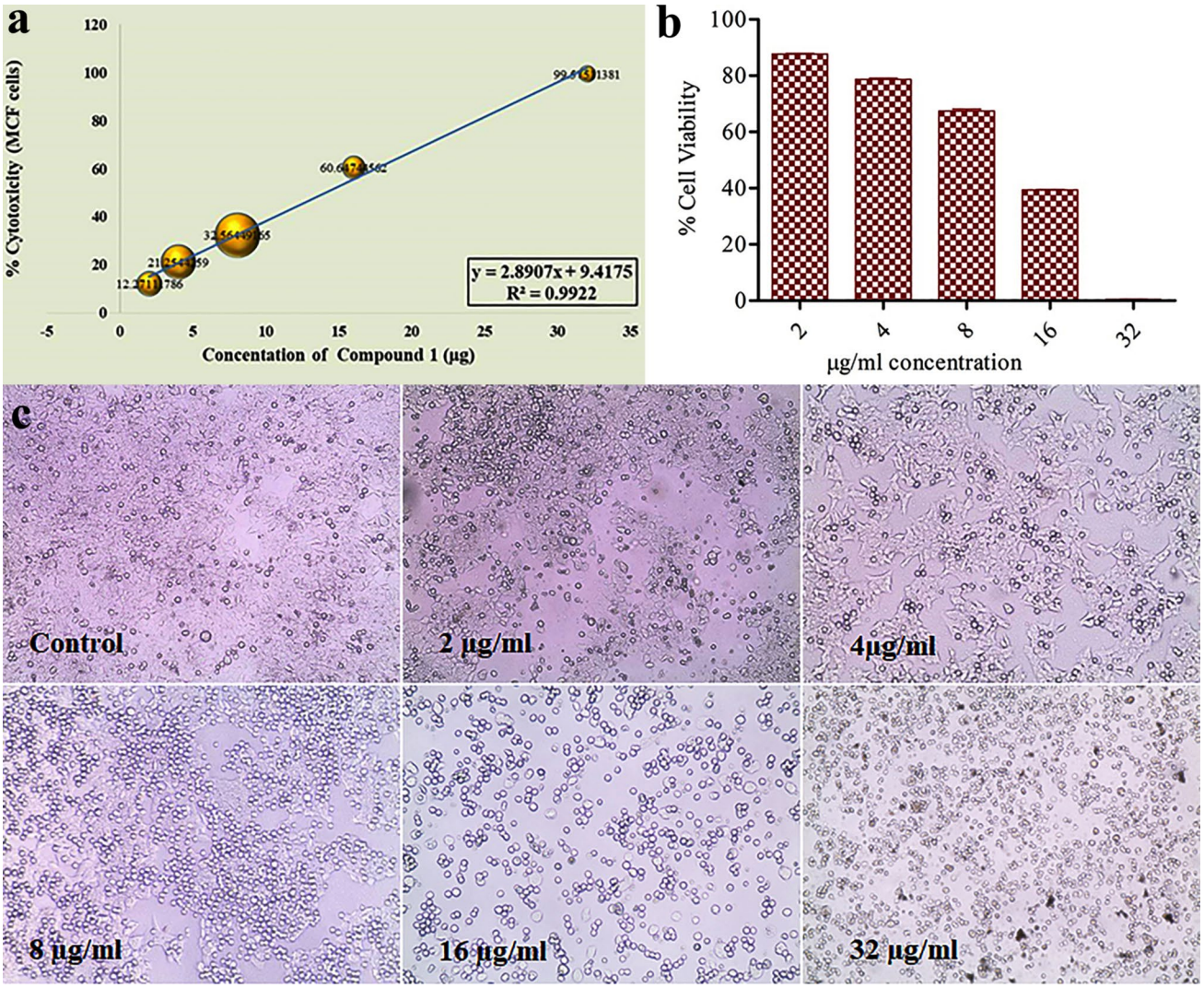

Fig. 10 The impact of compound 2a3 on the cytotoxic and apoptotic responses in MCF-7 breast adenoma cells was explored at varying dosages. the cytotoxicity levels (%) **a**, cell viability (%) **b**, and changes in apoptotic cell morphology in control **c**, 2 $\mu g \times mL^{-1}$, 4 $\mu g \times mL^{-1}$, 8 $\mu g \times mL^{-1}$, 16 $\mu g \times mL^{-1}$and 32 $\mu g \times mL^{-1}$

aniline 2a3, and the spectroscopic techniques were employed to characterize 4-((2-((3-nitrobenzylidene) amino)-4-phenyl-3,4,5,6-tetrahydro-7H-cyclopenta[d] pyrimidin-7-ylidene) methyl) aniline 2a3. This newly synthesized compound demonstrated effectiveness in molecular docking tests with various receptors, including 3LFF (Human p38 kinase), 5EW8 (Fibroblast growth factor receptor), 6E2N (MAPK), 6WW8 (CDK4/6 receptor), 7PCD (HER2), 7WT0 (human glyoxalase 1 receptor), and 8EXL (PI3K-alpha). Additionally, the compound 2a3 in vitro anti-breast cancer efficacy was notable, 2a3 exhibited an IC_{50} value of 14.03 µM/mL against MCF-7 cells against, where it exhibited significant anti-breast cancer activity that was straightforward and highly effective.

Experimental section

Materials

The starting compounds, reagents, and solvents utilized for synthesizing N-(7-(substituted benzylidene)-4-phenyl-4,5,6,7-tetrahydro-3H-cyclopenta[d]pyrimidin-2-yl)-1-(substituted phenyl)methanimine were of analytical grade or the finest quality available commercially. Melting points were determined using open capillary tubes without any correction. FT-IR spectra were obtained using KBr pellets and an ABB Bomem FT-IR spectrometer MB 104, supplied by ABB Limited in Bengaluru, India. Proton nuclear magnetic resonance (NMR) spectra were recorded with a Bruker 400 NMR analyser in Mumbai, India, utilizing Tetramethylsilane as the internal standard. Mass spectral data were acquired using a Shimadzu GC–MS QP 5000 quadrupole mass spectrometer in Chennai, India. Elemental microanalyses were performed using an Analysensysteme GmbH vario EL V300 elemental analyser. The purity of the chemicals was verified by thin-layer chromatography on pre-coated silica gel (HF254, 200 mesh) plates from E. Merck. The proposed structures were confirmed through IR, ^{1}H and ^{13}C-NMR, mass spectra, and chemical analysis studies.

Methods

Target identification

Targets for active components related to breast cancer were identified through several platforms, including Genecards, OMIM Swiss target prediction, Gprofiler, ShinyGO, and Venn diagrams. Venn diagrams are graphical representations that utilize overlapping circles to depict sets. They are handy for visually analysing and comparing different groups of components or variables linked to breast cancer. In these diagrams, overlapping circles for each type of breast cancer reveal common and unique risk factors [14–18].

Protein preparation

The structural data for various proteins was obtained from the Protein Data Bank (PDB), which is managed by the Research Collaboratory for Structural Bioinformatics (RCSB), accessible via (https://www.rcsb.org/). Specific identifiers from the database for 23 proteins include: 3WEJ (TACE), 5GIT (KEAP-1), 3VUC (Renin complex), 3WZE (VEGF receptor), 3ZR7 (Progesterone receptor), 5EW8 (Fibroblast growth factor receptor), 5LX6 (Human PARP inhibitor), 5U49 (Transthyretin receptor), 5WGD (Oestrogen receptor), 6E2N (MAPK), 6I6Z (Carboxypeptidase A1 receptor), 6QGG (Bcl-2 receptor), 6QUT (Carbonic anhydrase IX), 6S8L (Tubulin alpha receptor), 6WW8 (CDK4/6 receptor), 6XP1 (PYCR1), 7PCD (HER2), 7WT0 (human glyoxalase 1 receptor), 7XVZ (oestrogen receptor beta), 8A27 (EGFR), 8BWJ (ER-alpha), and 8EXL (PI3K-α). Before analysis, each protein was subject to preprocessing using the CHARMM-GUI program, which involved correcting for absent residues and eliminating unnecessary ligands and water molecules [14–18].

Ligand preparation

Seventy-five different compounds identified as N-(7-(substituted benzylidene)-4-phenyl-4,5,6,7-tetrahydro-3H-cyclopenta[d]pyrimidin-2-yl)-1-(substituted phenyl) methanimine, along with their corresponding cocrystals including 3WEJ (TACE), 5GIT (KEAP-1), 3VUC (Renin complex), 3WZE (VEGF receptor), 3ZR7 (Progesterone receptor), 5EW8 (Fibroblast growth factor receptor), 5LX6 (Human PARP inhibitor), 5U49 (Transthyretin receptor), 5WGD (Oestrogen receptor), 6E2N (MAPK), 6I6Z (Carboxypeptidase A1 receptor), 6QGG (Bcl-2 receptor), 6QUT (Carbonic anhydrase IX), 6S8L (Tubulin alpha receptor), 6WW8 (CDK4/6 receptor), 6XP1 (PYCR1), 7PCD (HER2), 7WT0 (human glyoxalase 1 receptor), 7XVZ (oestrogen receptor beta), 8A27 (EGFR), 8BWJ (ER-α), and 8EXL (PI3K-α), have shown potential activity against breast cancer. The ".sdp" data files for these compounds were sourced from the open-access PubChem database (https://pubchem.ncbi.nlm.nih.gov/). Each compound and cocrystal was analysed via the BIOVIA Discovery Studio Visualizer tool for cluster preparation https://discover.3ds.com/discovery-studio-visualizer-download [14–18].

Docking protocol

The AutoDock Vina-POAP virtual screening tool undertook several intermediary processes, such as creating pdbqt

formats for proteins and ligands. The configuration file encapsulated details about the protein and ligand and settings for the grid box dimensions. This application added polar hydrogens to the protein, solvation parameters and fragmental volumes. AutoGrid was responsible for constructing the grid map's box, the centre of which was defined by x, y, and z coordinates. A scoring grid was generated based on the ligand's structure to enhance computing speed. AutoDock Vina performs docking of proteins and ligands utilizing a method of iterated local search for global optimization under the assumption that their structures do not change. The outcomes displaying the lowest free energy of binding were compiled and displayed, omitting any results with a positional root mean square deviation more significant than 1.0A. The pose with the minimal binding affinity was selected for further analysis of amino acid interactions through BIOVIA Discovery Studio Visualizer. Proteins require a binding site for molecular attachment necessary for chemical reactions, including supporting catalytic areas to create sufficient residual sites for bioactive molecules. Both proteins and enzymes require specific binding sites to interact with target enzymes. PrankWeb (https://prankweb.cz/) identified all the target chemical active binding sites. Finally, AutoDock Vina-POAP virtual screening generated a receptor grid based on the protein's active site [14–18].

Molecular dynamics

A molecular dynamics simulation was carried out to assess the stability and variability of a protein–ligand interaction. This analysis aimed to determine how potential drug candidates bind to their respective protein targets. The simulations were executed using the Desmond module on a Linux system within the Maestro simulation framework by Schrödinger, Inc.. To manage the intricate protein–ligand interactions, the TIP3 water model was applied, establishing box-shaped boundaries. The system was balanced by adding Na + and Cl- salts in concentrations of 0.15 M. The NPT ensemble was used in the simulations to maintain a pressure of 1.01325 bar and a temperature of 300 K. Energy assessments employed the OPLS-4 force field, and data was recorded at 50-ps intervals. The simulation investigated complexes of **2a3** with proteins 3LFF (Human p38 kinase), 5EW8 (Fibroblast growth factor receptor), 6E2N (MAPK), 6WW8 (CDK4/6 receptor), 7PCD (HER2), 7WT0 (human glyoxalase 1 receptor), and 8EXL (PI3K-alpha) over 100 ns. The Desmond module in Schrödinger was used to analyse the MD simulation data meticulously. The study also incorporated techniques like the simulation interaction diagram to enhance analysis. The stability of the ligand–protein complexes was evaluated based on metrics such as root mean square deviation (RMSD), root mean square fluctuation (RMSF), and analysis of protein–ligand interactions in the simulated trajectories [14–18].

Density functionality theory

The referenced compounds include 4-((2-((3-nitrobenzylidene)amino)-4-phenyl-3,4,5,6-tetrahydro-7H-cyclopenta[d] pyrimidin-7-ylidene)methyl)aniline 2a3. Data files for these substances, specifically. SDP files were sourced from the PubChem public depository. These files were then processed using the Spartan14 graphical interface for energy minimization procedures. Additionally, GaussView 6.0.16 was utilized for the determination of the Hartree energy for the HOMO and LUMO orbitals [14–18]. The assessment of the energy gaps between HOMO and LUMO required the conversion of Hartree energy readings into electron-volt measurements, which serve as indicators of the molecular stability of compound 2a3.

ADMET modelling

We have evaluated the efficacy and robustness of compound 2a3 through in silico ADME (absorption, distribution, metabolism, and excretion studies and assessments of physicochemical properties. The SwissADME web service (http://www.swissadme.ch/) analysed parameters such as molecular weight, molar refractivity, solubility, bioavailability, and additional factors, including radar maps, the egg-boiled model, brain penetration, and human gastrointestinal absorption. SwissADME, accessible at no cost, enables researchers to predict pharmacokinetic properties and drug-likeness of test compounds and reference substances. The compound 4-((2-((3-nitrobenzylidene)amino)-4-phenyl-3,4,5,6-tetrahydro-7H-cyclopenta[d]pyrimidin-7-ylidene) methyl) aniline 2a3 was uploaded onto the SMARTCyp platform using SMILES notation. SMARTCyp's database stores data on molecules metabolized by CYP450 enzymes and includes precomputed energies of these molecules based on DFT activation https://smartcyp.sund.ku.dk/mol_to_som. Compound 2a3 was uploaded to the cardioToxCSM, which leverages advanced algorithms to provide critical insights into potential cardiac risks associated with molecular compounds. These include Arrhythmia, Cardiac Failure, Heart Block, hERG toxicity, Hypertension, and Myocardial Infarction. Serving as an essential tool in the field of cardiology https://biosig.lab.uq.edu.au/cardiotoxcsm/prediction [14–18].

Synthesis

The experiment commenced by mixing cyclopentanone 1 (0.01 mmol), substituted aromatic aldehyde (0.02 mmol), and guanidine hydrochloride (0.01 mmol) in a solution of sodium methoxide (0.01 mmol Na in 30 mL methanol) for 3 h. During this process, product precipitation was initiated by heating, followed by subsequent steps of filtration, washing with water, drying, and recrystallization, subsequently yielding 7-substituted benzylidene-4-phenyl-4,5,6,7-tetrahydro-3H-cyclopenta[d]pyrimidin-2-amine 1I. In the next phase of the experiment, the compound 1I (1.5 mmol), was dissolved in 7 mL of 96% ethanol. A 0.02 mmol amount of substituted benzaldehyde introduced into this solution. This mixture was subjected to reflux with constant stirring for 3 h. The product precipitated after the solution was left to rest at room temperature for 12 h at a temperature of + 4 °C. This final precipitate was processed through filtration, washed with water, dried, and recrystallized to yield the final compound 4-((2-((3-nitrobenzylidene)amino)-4-phenyl-3,4,5,6-tetrahydro-7H-cyclopenta[d]pyrimidin-7-ylidene)methyl) aniline 2a3.

MTT assay

The MCF-7 cell line, obtained from NCCS, was cultivated in DMEM medium enriched with 10% deactivated Fetal Bovine Serum (FBS), 100 IU/mL penicillin, and 100 µg/mL streptomycin under a humidity-controlled environment with 5% CO_2 at 37 °C until it reached confluency. Cells from the confluent monolayer were then trypsinized, and the cell density was adjusted to 1.0 × 10^5 cells/mL using the same medium formulation with 10% FBS. Subsequently, 100 µL of this cell suspension (1 × 10^4 cells/well) was introduced into each well of a 96-well microtiter plate. After 24 h, once a partial monolayer had formed, the supernatant was discarded, and the cells were washed once with the medium. Various concentrations of test samples were then applied to the cells at 100 µL per well, and the plate was incubated for a further 24 h at 37 °C in a 5% CO_2 environment. Following this incubation period, the test solutions were removed, and 20 µL of MTT solution (2 mg/mL MTT in PBS) was introduced to each well. The plate was then incubated for four hours at the same temperature and CO_2 conditions. Post-incubation, the supernatant was aspirated, and 100 µL of DMSO was added. The plate was agitated gently to dissolve the resulting formazan. Absorbance at 570 nm was measured using a microplate reader to determine cell viability [19, 20]. The viability percentage was computed using the formula: % viability = (Sample abs/Control abs × 100).

Supplementary Information The online version contains supplementary material available at https://doi.org/10.1007/s13738-024-03169-6.

Acknowledgements We would like to extend our heartfelt gratitude to the management and administration of School of Pharmaceutical Sciences Vels Institute of Science Technology & Advanced Studies, Pallavaram, Chennai, Tamilnadu-600117, India for providing all of the essential facilities for lead compounds synthesis. The authors gratefully acknowledge the chemistry department at Pacific Academy of Higher Education and Research University, Pacific Hills, Pratapnagar Extn., Airport Road, Debari, Udaipur, India.

Author contributions TP, MS, and AM contributed to the study's conception and design. PP and SK performed synthesis and computational simulation and analysed the data. TP, SK, GS, and AM wrote the original manuscript. TP and SK proofread it. All the authors have read and approved the manuscript for submission.

Declarations

Conflict of interest The authors declare that they have no known competing financial interests or personal relationships that could have appeared to influence the work reported in this paper.

Ethical approval None of the authors conducted any human or animal experiments for this publication.

References

1. A. Yadav, E.R. Rene, M.K. Mandal, K.K. Dubey, Chemosphere **263**, 128285 (2021)
2. S. Cherukupalli, G.A. Hampannavar, S. Chinnam, B. Chandrasekaran, N. Sayyad, F. Kayamba, R.R. Aleti, R. Karpoormath, Bioorg. Med. Chem. **26**, 309–339 (2018)
3. S. Mohana Roopan, R. Sompalle, Synth Commun **46**, 645–672 (2016)
4. I. Rani, N. Kaur, A. Goyal, M. Sharma, Anti-Cancer Agents Med. Chem. **23**, 525–561 (2023)
5. A. Alsharif, M. Allahyani, A. Aljuaid, A.A. Alsaiari, M.M. Almehmadi, M. Asif, Curr. Org. Chem. **27**, 1779–1798 (2023)
6. N. Tong, Duquesne University, (2022)
7. D.J. Baillache, A. Unciti-Broceta, RSC Med. Chem. **11**, 1112–1135 (2020)
8. J. Basha, N.M. Goudgaon, J. Mol. Struct. **1246**, 131168 (2021)
9. E.V. Filho, E.M.C. Pinheiro, S. Pinheiro, S.J. Greco, Tetrahedron **92**, 132256 (2021). https://doi.org/10.1016/j.tet.2021.132256
10. T. Panneerselvam, J.R. Mandhadi, J. Heterocycl. Chem. **57**, 3082–3088 (2020)
11. P.G. Dessai, S.P. Dessai, R. Dabholkar, P. Pednekar, S. Naik, S. Mamledesai, M. Gopal, P. Pavadai, B.K. Kumar, S. Murugesan, Mol. Divers. **27**, 1567–1586 (2023)
12. T. Panneerselvam, V. Sivakumar, S. Arumugam, K. Selvaraj, M. Indhumathy, Drug Res **67**, 289–301 (2017)
13. T.P. Selvam, C.R. James, P.V. Dniandev, S.K. Valzita, Res. Pharm. **2**, 1–9 (2015)
14. J.R. Mandhadi, T. Panneerselvam, P. Parasuraman, Curr. Bioact. Compd. **16**, 294–301 (2020)
15. C. Palanichamy, P. Pavadai, T. Panneerselvam, S. Arunachalam, E. Babkiewicz, S. Ram Kumar Pandian, K. Shanmugampillai Jeyarajaguru, D. Nayak Ammunje, S. Kannan, J. Chandrasekaran, Molecules **27**, 3799 (2022)
16. T. Panneerselvam, S. Kunjiappan, S. Govindaraj, M. Gopal, K. Natarajan, Y.M. Hegde, N. Shanmugam, G. Srinivas, K. Ravi, V.

Natarajan, Anti-Cancer Agents Med. Chem. (2022). https://doi.org/10.2174/1871520623666221205140328
17. R.R. Rajeshkumar, B.K. Kumar, P. Parasuraman, T. Panneerselvam, K. Sundar, D.N. Ammunje, S.R.K. Pandian, S. Murugesan, S.J. Kabilan, S. Kunjiappan, BioImpacts **12**, 487 (2022)
18. G. Saravanan, T. Panneerselvam, S. Kunjiappan, P. Parasuraman, V. Alagarsamy, P. Udayakumar, M. Soundararajan, S.D. Joshi, S. Ramalingam, D.N. Ammunje, Drug Dev. Res. **80**, 368–385 (2019)
19. A.K. Kalimuthu, P. Pavadai, T. Panneerselvam, E. Babkiewicz, J. Pijanowska, P. Mrówka, G. Rajagopal, V. Deepak, K. Sundar, P. Maszczyk, Molecules **27**, 8814 (2022)
20. R.R. Rajeshkumar, P. Pavadai, T. Panneerselvam, S.R.K. Pandian, A.S.K. Kumar, P. Maszczyk, E. Babkiewicz, S.J. Kabilan, S. Kunjiappan, J. Environ. Polym. Degrad. **32**(5), 2120–2139 (2023)

Authors and Affiliations

Arunkumar Manoharan[1] · Panneerselvam Theivendren[2] · Maya Sharma[1] · Selvaraj Kunjiappan[3] · Saravanan Govindaraj[2] · Parasuraman Pavadai[4]

✉ Panneerselvam Theivendren
tpsphc@gmail.com

✉ Maya Sharma
maya.sharma1703@gmail.com

[1] Department of Pharmaceutical Chemistry, Faculty of Pharmacy, Pacific Academy of Higher Education and Research University, Pacific Hills, Pratapnagar Extn., Airport Road, Debari, Udaipur 313003, India

[2] Department of Pharmaceutical Chemistry & Analysis, School of Pharmaceutical Sciences, Vels Institute of Science, Technology & Advanced Studies, Pallavaram, Chennai, Tamilnadu 600117, India

[3] Department of Biotechnology, Kalasalingam Academy of Research and Education, Tamil Nadu, Krishnankoil 626126, India

[4] Department of Pharmaceutical Chemistry, Faculty of Pharmacy, M.S. Ramaiah University of Applied Sciences, M S R Nagar, Bengaluru, Karnataka 560054, India